Defence Research and Development Canada
Recherche et développement pour la défense Canada

DEFENCE R&D DÉFENSE

Focusing ISAR Images using the Adaptive Local Polynomial Fourier Transform

T. Thayaparan

Defence R&D Canada – Ottawa
TECHNICAL MEMORANDUM
DRDC Ottawa TM 2006-185
September 2006

Canada

Focusing ISAR Images using the Adaptive Local Polynomial Fourier Transform

T. Thayaparan
Defence R&D Canada – Ottawa

Defence R&D Canada – Ottawa

Technical Memorandum

DRDC Ottawa TM 2006-185

September 2006

Abstract

The adaptive local polynomial Fourier transform is employed for the improvement of the ISAR images in complex reflector geometry cases, as well as in cases of fast maneuvering targets. It has been shown that this simple technique can produce significantly improved results with a relatively modest calculation burden. Two forms of the adaptive LPFT are proposed. The adaptive parameter in the first form is calculated for each radar chirp. An additional refinement is performed by using the information from the adjacent chirps. The second technique is based on the determination of the adaptive parameter for different parts of the radar image. The numerical analysis demonstrates the accuracy of the proposed techniques. It is important to note that the proposed technique does not assume any particular model of radar target motion. It can be applied for any realistic motion of targets.

Résumé

La transformée de Fourier polynomiale locale (TFPL) adaptative est ici utilisée pour améliorer les images ISAR dans le cas de réflecteurs à géométrie complexe et de cibles effectuant des manoeuvres rapides. Il a été démonté que cette technique simple améliore sensiblement les résultats au prix d'un effort de calcul relativement modeste. Deux formes de la TFPL adaptative sont proposées. Le paramètre adaptatif de la première forme est calculé pour chaque impulsion comprimée radar. Le résultat est raffiné à l'aide de l'information provenant des impulsions comprimées adjacentes. La deuxième technique se fonde sur la détermination du paramètre adaptatif pour différentes parties de l'image radar. L'analyse numérique montre l'exactitude des techniques proposées. Notons que la technique proposée ne suppose aucun modèle particulier de mouvement de cible radar. Elle est applicable à tout mouvement de cible réaliste.

This page intentionally left blank.

Executive summary

The Inverse Synthetic Aperture Radar (ISAR) is a technique for forming high-resolution images by utilizing the information inherent in the differential target Doppler that results from rotation of an object (the target) relative to the radar. Its applications include imaging and discrimination of ships and aircraft with airborne or land based radar systems.

Polarimetric SAR/ISAR imaging is an effective way to acquire high resolution images of targets of interest at long range and as such is an irreplaceable tool in the task of non-cooperative target recognition of both ships and ground moving targets. One of the significant problems with SAR/ISAR image formation of a moving target is the assumption of time invariance of the Doppler frequency used to resolve the image in the cross range. Time variant Doppler becomes present in a SAR signal when a moving target is maneuvering, or a ship is pitching and rolling during the coherent processing interval and is typically referred to as motion error. Using the fast Fourier transform to cross range focus an image with this motion error present will cause extensive blurring in the cross range and leave the image unrecognizable even to the most experienced SAR operators. The aim of this report is to compensate for the target motion, to generate an image equivalent to that of the stationary target.

The Canadian Air Force is currently upgrading her fleet of CP-140 Aurora maritime patrol aircraft to possess NCTR through ISAR in order to increase the capability of the Canadian Forces in both sovereignty patrols of Canadian territory and the protection of the Canadian Patrol Frigates and allied ships operating abroad as a coalition. The United States Navy's equivalent aircraft, the P-3 Orion, currently possesses this capability. Therefore, effective ISAR imaging will have a real impact in the decision making process in future military operations involving both Canadian and American forces.

In this report the adaptive local polynomial Fourier transform is employed for improvement of the ISAR images in complex reflector geometry cases, as well as in cases of fast maneuvering targets. It has been shown that this simple technique can produce significantly improved results with a relatively modest calculation burden. Two forms of the adaptive LPFT are proposed. The adaptive parameter in the first form is calculated for each radar chirp. The additional refinement is performed by using the information from the adjacent chirps. The second technique is based on the determination of the adaptive parameter for different parts of the radar image. The numerical analysis demonstrates the accuracy of the proposed techniques. It is important to note that the proposed technique does not assume any particular model of radar target motion. It can be applied for any realistic motion of targets.

T. Thayaparan; 2006; Focusing ISAR Images using the Adaptive Local Polynomial Fourier Transform; DRDC Ottawa TM 2006-185; Defence R&D Canada – Ottawa.

Sommaire

La technique ISAR (radar à synthèse d'ouverture inverse) permet de former des images à haute résolution à l'aide de l'information inhérente du Doppler différentiel de cible que produit la rotation d'un objet (la cible) par rapport au radar. Ses applications comprennent l'imagerie et la discrimination de navires et d'aéronefs au moyen de systèmes radar aéroportés ou basés au sol.

Moyen efficace d'acquérir des images à haute résolution de cibles d'intérêt à longue distance, l'imagerie polarimétrique SAR/ISAR est un outil irremplaçable pour la reconnaissance de cibles non coopératives (NCTR), y compris les navires et les cibles au sol. Un problème important de la formation d'images de cible SAR/ISAR tient à ce que la fréquence Doppler utilisée pour résoudre l'image mobile en portée latérale est censée être invariable dans le temps. La fréquence Doppler d'un signal SAR commence à varier dans le temps lorsqu'une cible mobile effectue des manoeuvres, ou en présence de roulis et de tangage pendant l'intervalle de traitement cohérent. On parle alors généralement d'" erreur de mouvement ". L'utilisation de la transformée de Fourier rapide pour mettre au point l'image en portée latérale présentant cette erreur de mouvement produit un important brouillage de la portée latérale et rend l'image méconnaissable même à l'opérateur SAR le mieux averti. Le présent rapport étudie comment compenser le mouvement de la cible afin d'obtenir une image équivalant à celle de la cible immobile.

La Force aérienne du Canada est en train de mettre à niveau la flotte d'avions de patrouille maritime CP-140 Aurora en les dotant de la fonction NCTR au moyen de l'ISAR afin d'augmenter la capacité des Forces canadiennes tant dans les patrouilles de protection de la souveraineté du territoire canadien que dans la protection des frégates de patrouille canadiennes et des navires alliés faisant partie d'une coalition à l'étranger. L'aéronef équivalent de la marine américaine, le P-3 Orion, est déjà doté de cette capacité. Par conséquent, une imagerie ISAR efficace aura une forte incidence sur le processus de prise de décisions lors d'opérations militaires futures effectuées par des forces canadiennes et américaines.

La transformée de Fourier polynomiale locale (TFPL) adaptative est ici utilisée pour améliorer les images ISAR dans le cas de réflecteurs à géométrie complexe et de cibles effectuant des manoeuvres rapides. Il a été démonté que cette technique simple améliore sensiblement les résultats au prix d'un effort de calcul relativement modeste. Deux formes de la TFPL adaptative sont proposées. Le paramètre adaptatif de la première forme est calculé pour chaque impulsion comprimée radar. Le résultat est raffiné à l'aide de l'information provenant des impulsions comprimées adjacentes. La deuxième technique se fonde sur la détermination du paramètre adaptatif pour différentes parties de l'image radar. L'analyse numérique montre l'exactitude des techniques proposées. Notons que la technique proposée ne sup-

pose aucun modèle particulier de mouvement de cible radar. Elle est applicable à tout mouvement de cible réaliste.

T. Thayaparan; 2006; Focusing ISAR Images using the Adaptive Local Polynomial Fourier Transform; DRDC Ottawa TM 2006-185; R & D pour la défense Canada – Ottawa.

Table of contents

List of figures

This page intentionally left blank.

1 Introduction

The inverse synthetic aperture radar (ISAR) has attracted wide interest within scientific and military community. Some ISAR applications are already well known and studied. However, many important issues remain to be addressed. For example, suitable enhancement techniques for the fast maneuvering radar targets or targets with fast moving parts is not yet known. Also, the standard approaches based on the Fourier transform (FT) fail to resolve the influence of closely spaced reflectors. There are several techniques for improvement of the ISAR radar image in the case of fast maneuvering targets or in the case of objects with complex reflector geometry. Here we mention only two groups of such enhancement techniques:

- techniques that adapt transform parameters for assumed parametric target motion model [1, 6];

- techniques where reflection signal components are parametrized, while the signal components caused by reflectors are estimated by using some of the well developed parametric spectral estimation tools [2, 3].

Both of these techniques have some advantages, but they also have some drawbacks for specific applications. The first group of techniques is strongly based on the radar target geometry with an assumed motion model. These techniques could become inaccurate in the case of a changing motion model. The second group of techniques is tested on simulated examples. However, its application in real scenarios, where signal components are caused by numerous scatterers, could be very difficult. Namely, there are no appropriate methods for parameter estimation of signals with a very large number of components.

In this report we propose a modification of the first group of research techniques. The adaptive local polynomial Fourier transform (LPFT) is used. The adaptive coefficients are calculated for each considered chirp in the radar signal mixture. It is important to note that the proposed technique does not assume any particular model of radar target motion. The adaptive parameters are estimated for each scattering point independently. Based on the analysis of the signal obtained from the target we consider some simplifications in the process of calculation of the adaptive transform. In this way we keep the calculation burden to within reasonable limits. The two techniques for the enhancement of the radar image by using the LPFT are considered. The first one is based on the information obtained from each chirp separately and on the possible refinement by combining results from various chirps. The second technique is based on the detection of regions-of-interest in the range/cross-range plane and on the determination of the optimal LPFT for each detected region [19].

The report is organized as follows: The target and radar signal modeling is discussed in Section 2. The proposed methods are introduced in Section 3. The simulation study is given in Section 4. The conclusions are given in Section 5.

2 Radar Signal Model

Consider a radar signal consisting of M continuous wave coherent pulses:

$$v_M(t) = \sum_{m=0}^{M-1} v_0(t - mT_r), \tag{1}$$

where $v_0(t)$ is the basic impulse limited within the interval $-T_r/2 \leq t < T_r/2$. The linear frequency modulated (FM) signal is used in our simulations as a basic impulse: $v_0(t) = \exp(j\pi Bt^2/T_r)$, where B is the bandwidth control parameter while T_r is the pulse repetition time. The alternative radar model used in practice has radar pulses with stepped frequencies, however, this model is not studied in this report. The defocusing effect considered in this report and time-frequency (TF) signatures of the obtained radar signals have similar behavior for these two forms of radar signals [4, 5].

The signal emitted toward the radar target can be written as:

$$u(t) = e^{j2\pi f_0 t} v_M(t), \tag{2}$$

where f_0 is the radar operating frequency. The received signal, reflected from a single reflector target at distance $d(t)$, is delayed for $2d(t)/c$, with σ being the reflection coefficient and c being the propagation rate:

$$u_R(t) = \sigma u\left(t - 2d(t)/c\right). \tag{3}$$

The demodulation of the received signal can be performed by multiplying the received with the transmitted signal $u(t)$:

$$q(t) = \sigma u^*(t - 2d(t)/c)u(t) =$$

$$\sigma \exp(j4\pi f_0 d(t)/c) \sum_{m=0}^{M-1} v_0^*(t - 2d(t)/c - mT_r) \sum_{m=0}^{M-1} v_0(t - mT_r - T_0). \tag{4}$$

The parameter T_0 is used in radar imaging for compensation of target distance. For properly selected T_0 and after highpass filtering, the signal $q(t)$ can be approximately written as:

$$q(t) \approx \sigma \exp(j4\pi f_0 d(t)/c) \sum_{m=0}^{M-1} v_0^*(t - 2d(t)/c - mT_r) v_0(t - mT_r) = \sum_{m=0}^{M-1} q(m,t), \tag{5}$$

where

$$\begin{aligned} q(m,t) &= \sigma \exp(j4\pi f_0 d(t)/c) v_0^*(t - 2d(t)/c - mT_r) v_0(t - mT_r), \\ &t \in [(m - 1/2)T_r, (m + 1/2)T_r), \\ &= \sigma \exp(j4\pi f_0 d(t)/c) \exp(j4\pi B d(t)(t - mT_r)/(cT_r)) \exp(-j\pi B(2d(t)/c)^2/T_r). \end{aligned} \tag{6}$$

Keeping in mind that $B \ll f_0$, we can neglect $\exp(-j\pi B(2d(t)/c)^2/T_r)$ with respect to the other two components. The value of $q(m,t)$ can approximately be written as:

$$q(m,t) \approx \sigma \exp(j4\pi f_0 d(t)/c) \exp(j4\pi B d(t)(t - mT_r)/(cT_r)). \tag{7}$$

This signal is commonly given in the form:

$$q(m,\tau) \approx \sigma \exp(j4\pi f_0 d(\tau + mT_r)/c) \exp(j4\pi B d(\tau + mT_r)\tau/(cT_r)), \tag{8}$$

where $t = \tau + mT_r$. Parameter $\tau \in [-T_r/2, T_r/2)$ is referred to as fast-time, while $m = 0, 1, ..., M-1$, is called the slow-time coordinate. Commonly, in actual radar systems, signals are discretized in fast-time coordinate with sampling rate $T_s = T_r/N$, $\tau = nT_s$, where $n \in [-N/2, N/2)$. The classical radar setup assumes that the radar target position is a linear function of time $d(t) = D_0 + Vt$. Then the radar model produces:

$$q(m,\tau) \approx \sigma \exp(j4\pi f_0 D_0/c) \exp(j4\pi V m f_0 T_r/c) \exp(j4\pi\tau B D_0/(cT_r)). \tag{9}$$

A two-dimensional (2D) FT of this signal over m and τ is approximately:

$$Q(\omega_\tau, \omega_m) = \int_\tau \sum_{m=0}^{M-1} q(m,\tau) e^{-j\omega_\tau \tau - j\omega_m m} d\tau \approx$$

$$\int_{\tau}\sum_{m=0}^{M-1}\sigma\exp(j4\pi f_0 D_0/c)\exp(j4\pi V m f_0 T_r/c)\exp(j4\pi\tau B D_0/(cT_r))e^{-j\omega_\tau\tau-j\omega_m m}d\tau$$

$$=\sigma\exp(j4\pi f_0 D_0/c)\int_{\tau}\exp(j4\pi\tau B D_0/(cT_r))e^{-j\omega_\tau\tau}d\tau\sum_{m=0}^{M-1}\exp(j4\pi V m f_0 T_r/c)e^{-j\omega_m m}$$

$$=(2\pi)\sigma\exp(j4\pi f_0 D_0/c)\delta(\omega_\tau-4\pi B D_0/(cT_r))\frac{\sin((\omega_m-4\pi V f_0 T_r/c)M/2)}{\sin((\omega_m-4\pi V f_0 T_r/c)/2)}$$

$$\times e^{-j(\omega_m-4\pi V f_0 T_r/c)(M-1)/2}. \tag{10}$$

$$|Q(\omega_\tau,\omega_m)|=|(2\pi)\sigma\exp(j4\pi f_0 D_0/c)\delta(\omega_\tau-4\pi B D_0/(cT_r))$$
$$\times\frac{\sin((\omega_m-4\pi V f_0 T_r/c)M/2)}{\sin((\omega_m-4\pi V f_0 T_r/c)/2)}e^{-j(\omega_m-4\pi V f_0 T_r/c)(M-1)/2}$$
$$=|2\pi||\sigma||\exp(j4\pi f_0 D_0/c)||\delta(\omega_\tau-4\pi B D_0/(cT_r))|\left|\frac{\sin((\omega_m-4\pi V f_0 T_r/c)M/2)}{\sin((\omega_m-4\pi V f_0 T_r/c)/2)}\right|\times|e^{-j(\omega_m-4\pi V f_0 T_r/c)(M-1)/2}| \tag{11}$$
$$=|(2\pi)\sigma\delta(\omega_\tau-4\pi B D_0/(cT_r))\frac{\sin((\omega_m-4\pi V f_0 T_r/c)M/2)}{\sin((\omega_m-4\pi V f_0 T_r/c)/2)}|$$
$$\approx(2\pi)\sigma\delta(\omega_\tau-4\pi B D_0/(cT_r))M\delta(\omega_m-4\pi V f_0 T_r/c)$$

since

$$\frac{\sin(\alpha M)}{\sin(\alpha)}\approx M\delta(\alpha)$$

for relatively large M.

Therefore, for large M we can write the magnitude of $Q(\omega_\tau,\omega_m)$ as:

$$|Q(\omega_\tau,\omega_m)|\approx(2\pi)\sigma\delta(\omega_\tau-4\pi B D_0/(cT_r))M\delta(\omega_m-2V f_0 T_r/c). \tag{12}$$

The distance can be approximately written as $d(t)\approx R(t)+x_p\cos(\theta(t))+y_p\sin(\theta(t))$, where $R(t)$ is the distance of the target rotation center from the radar, where coordinates of the scatterer, for $\tau=0$, are (x_p,y_p) (see Figure 1). The coordinate system is formed in such a way that the coordinate x is the line of sight. Assume constant rotation velocity $\theta(t)=\omega_R t$, with relatively small angular movement of the target $|\omega_R T_r|\ll 1$ (it implies that $\cos(\theta(t))\approx 1$ and $\sin(\theta(t))\approx 0$). According to the introduced conditions $d(t)\approx x_p$ and $v(t)=d'(t)=-x_p\theta'(t)\sin(\theta(t))+y_p\theta'(t)\cos(\theta(t))\approx y_p\theta'(t)\cos(\theta(t))\approx y_p\omega_R$. Commonly, it is assumed that $R(t)$ is

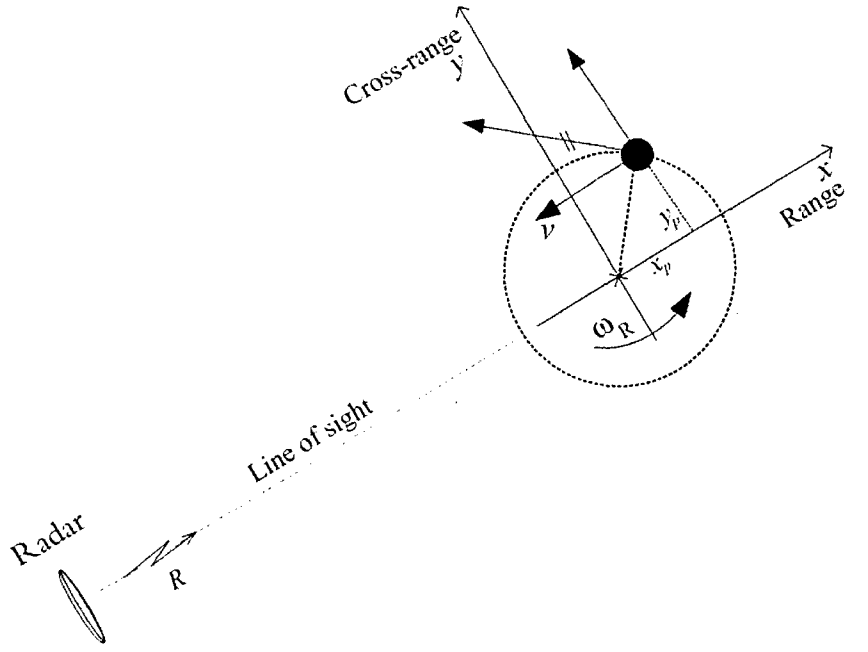

Figure 1: *Illustration of the radar target geometry.*

compensated by adjusting T_0 in (4). Thus, we will not consider it in our algorithm. Then $|Q(\omega_\tau, \omega_m)|$ can be written as:

$$\begin{aligned} |Q(\omega_\tau, \omega_m)| &\approx (2\pi)\sigma M \delta(\omega_\tau - 4\pi B x_p/(cT_r))\delta(\omega_m - 4\pi y_p \omega_R f_0 T_r/c) \\ &= (2\pi)\sigma M \delta(\omega_\tau - c_1 x_p)\delta(\omega_m - c_2 y_p). \end{aligned} \tag{13}$$

It represents the ISAR image of scatterer (x_p, y_p) for a given instance under introduced assumptions. Note that the constants that determine the resolution of the radar image are given by $c_1 = 4\pi B/(cT_r)$ and $c_2 = 4\pi\omega_R f_0 T_r/c$. The radar image is formed as a superposition of radar images of all scatterers (x_p, y_p), $p = 1, 2, ..., P$. It is approximately given as:

$$|Q(\omega_\tau, \omega_m)| = \sum_{p=1}^{P} (2\pi)\sigma_p \delta(\omega_\tau - c_1 x_p)\delta(\omega_m - c_2 y_p), \tag{14}$$

where σ_p is the reflection coefficient that corresponds to the p-th scatterer point.

In numerous cases we cannot assume that the radar model can be simplified in the previously described manner. For example, the radar target can be very fast, or the

model of radar target motion can be more complicated (for example 3D motion). Then, instead of complex sinusoids given by (9), the polynomial phase of the radar signal model can be written as,

$$q(m,\tau) = \sigma_p \exp\left(j \sum_{l=0}^{L} a_{m,l}\tau^l/l!\right), \tag{15}$$

where parameters $a_{m,l}$ depend on the considered chirp and scatterer motion. For example, for the target motion model $d(t) = D_0 + V_0 t + At^2/2$, where A is acceleration of the target, the coefficients $a_{m,l}$ are approximately calculated as follows.

Start with the Equation (8), $q(m,\tau) \approx \sigma \exp(j4\pi f_0 d(\tau + mT_r)/c) \exp(j4\pi B d(\tau + mT_r)\tau/(cT_r))$, and introduce $d(t) = D_0 + V_0 t + At^2/2$:

$$q(m,\tau) \approx \sigma \exp(\frac{j4\pi f_0}{c}[D_0 + V_0(\tau + mT_r) + A(\tau + mT_r)^2/2])$$
$$\times \exp\left(\frac{j4\pi B}{(cT_r)}[D_0 + V_0(\tau + mT_r) + A(\tau + mT_r)^2/2]\tau\right).$$

Coefficients $a_{m,l}$ are approximately equal to

$$a_{m,0} = \frac{4\pi f_0}{c}[D_0 + V_0 mT_r + A(mT_r)^2/2],$$

terms with τ are

$$a_{m,1} = \frac{4\pi f_0}{c}[V_0 + AmT_r] + \frac{4\pi B}{(cT_r)}[D_0 + V_0 mT_r + A(mT_r)^2/2],$$

terms with τ^2 are

$$a_{m,2} = \frac{8\pi}{c}\left(f_0\frac{A}{2} + B\frac{V_0}{T_r} + Am\right),$$

terms with τ^3 are

$$a_{m,3} = \frac{12\pi BA}{cT_r}, \tag{16}$$

and $a_{m,l} = 0$ for $l > 3$. Some terms of these coefficients can be ignored, but in general it is not as simple as in the case when we can assume that the scatterer position is a linear function. The situation becomes even more difficult in the case when the target model is not a simple rotating model. When the target model is complex, a very complicated relationship between the position of scatterers (x_p, y_p) and the coefficients of the polynomial in the signal phase can be established. Also, the polynomial that should be used to accurately estimate the signal phase will be

of very high order. The radar image obtained by using the 2D FT of the signal with higher order polynomial becomes spread (defocused) in the range/cross-range domain (ω_τ, ω_m). The goal of the ISAR signal processing is to obtain the focused radar image, i.e., to remove the influence of the higher order polynomial in signal phase of each component.

Usually, it is assumed that the modeling of coefficients is possible based on the target motion model. In this case, instead of all possible parameters, only parameters of the motion model should be used in order to perform an enhancement of the radar image.

The first group of techniques for the enhancement of radar images is based on this concept. One such approach is described in [6] where it is assumed that the radar target scatterers can be modeled with a relatively simple motion model which assumes that the velocity increases or decreases linearly (or that angular velocity changes in linear manner) within the repetition time. After estimating the acceleration of the target, the variation in the velocity is compensated from the signal and finally a focused radar image is obtained. It corresponds to removing the influence of acceleration from (15). However, these techniques are very sensitive to any variations from the assumed motion model. They cannot be used for 3D motion models.

Alternative techniques are based on estimation of all the $a_{m,l}$ coefficients in the polynomial phase of the received signal [2, 3]. These techniques are usually based on iteration, removing of the lower order coefficients from the signal phase in order to estimate the highest order coefficient. Then, the estimation of lower order coefficients is performed by using the same procedure but for the dechirped signal. It means that the error in the estimation of the highest order coefficient propagates toward the lower order coefficients. Furthermore, it has recently been shown that these procedures are biased for multicomponent signals and that the dechirping procedure used to produce a signal suitable for estimation of the lower order coefficients introduces an additional source of errors for multicomponent signals. These techniques are also time consuming and, as far as we know, never applied to signals with a large number of components. Numerous components caused by target scatterers could appear in the radar signal.

A novel technique for enhancing radar images, that introduces just one new adaptive parameter in the FT expression for each received signal, is introduced in the next section. For each chirp, only one parameter of the transform should be estimated. The second important property of this technique is in the fact that we do not assume any particular target motion model. Therefore it can be applied for any realistic motion of targets.

3 Adaptive Local Polynomial FT

In this section we introduce the LPFT as a tool for the autofocusing of ISAR images. Two forms of the adaptive LPFT are proposed. The first form can be applied to each chirp component separately with possible refinements by using information from the adjacent chirps (Section 3.1). The second form performs evaluation of the adaptive LPFT for each detected region-of-interest in the radar image (Section 3.2).

3.1 First form: Adaptive LPFT for radar signals

In order to develop this approach we will go through several typical cases of signals, starting from a very simple case to the much more complicated cases. The improvement in signal components concentration (focusing radar image) is performed by estimating the signal parameters without assuming any particular motion model. This is a quite different approach compared to the methods with predefined motion model or to the methods where estimation is performed on each parameter $a_{m,l}$.

3.1.1 Linear FM signal case

The simplest case of monocomponent linear FM signal

$$q(m,\tau) = \sigma \exp\left(j[a_{m,0} + a_{m,1}\tau + a_{m,2}\tau^2/2]\right) \tag{17}$$

is considered first. In this case, the dependence on m in parameter indices will be removed for the sake of notation brevity. Then, the signal can be written as:

$$q(m,\tau) = \sigma \exp\left(j[a_0 + a_1\tau + a_2\tau^2/2]\right) \tag{18}$$

For the analysis of these kind of signals, we can use the LPFT [7], [8]:

$$F(\omega_\tau, m; \alpha) = \int_{-\infty}^{\infty} q(m,\tau)w(\tau)\exp(-j\alpha\tau^2/2)\exp(-j\omega_\tau\tau)d\tau, \tag{19}$$

where $w(\tau)$ is a window function of the width T_w, $w(\tau) = 0$ for $|\tau| \geq T_w/2$.

The LPFT is ideally concentrated along the instantaneous frequency for $\alpha = a_2$:

$$F(\omega_\tau, m; a_2) = \sigma \int_{-\infty}^{\infty} w(\tau)\exp\left(j[a_0 + a_1\tau + a_2\tau^2/2]\right) \times$$

$$\exp(-j\omega_\tau\tau - ja_2\tau^2/2)d\tau$$
$$= \sigma e^{ja_0}\int_{-\infty}^{\infty} w(\tau)\exp(-j(\omega_\tau - a_1))d\tau$$
$$= \sigma e^{ja_0}W(\omega_\tau - a_1) \tag{20}$$

where $W(\omega_\tau) = FT\{w(\tau)\}$. Function $F(\omega_\tau, m; a_2)$ is highly concentrated around $\omega_\tau = a_1$, since the FT of common wide window functions (rectangular, Hamming, Hanning, Gauss) is highly concentrated around the origin (in our simulations the window width is equal to the repetition rate $T_w = T_r$). The radar image can be obtained from $F(\omega_\tau, m; a_2)$ by evaluating the 1D FT along the $m-$coordinate axis:

$$Q(\omega_\tau, \omega_m; a_2) = \sum_{m=0}^{M-1} F(\omega_\tau, m; a_2)e^{-j\omega_m m}. \tag{21}$$

3.1.2 Higher order polynomial FM signal

For the higher order polynomial signal:

$$q(m, \tau) = \sigma\exp\left(j\phi_m(\tau)\right) = \sigma\exp(j\phi(\tau)) \tag{22}$$

the LPFT can be written as:

$$F(\omega_\tau, m; \alpha) = \int_{-\infty}^{\infty} \sigma\exp(j\phi(\tau))w(\tau)\exp(-j\alpha\tau^2/2)\exp(-j\omega_\tau\tau)d\tau$$

$$= \sigma\int_{-\infty}^{\infty}\exp(j\phi(0) + j\phi'(0)\tau + j\phi''(0)\tau^2/2 + j\phi'''(0)\tau^3/3! + ...$$
$$+j\phi^{(n)}(0)\tau^n/n! + ... - j\alpha\tau^2/2 - j\omega_\tau\tau)w(\tau)d\tau \tag{23}$$

For $\phi^{(n)}(0) = 0$ for $n > 2$ we obtain a highly concentrated LPFT for $\alpha = \phi''(0)$:

$$F(\omega_\tau, m; \phi''(0)) = \sigma\exp(j\phi(0))W(\omega_\tau - \phi'(0)) \tag{24}$$

The second derivative of the signal phase is commonly called chirp-rate parameter.

In the case when higher order derivatives are non-zero, the LPFT will not be ideally concentrated and there will be some spread in the frequency domain caused by the

FT of terms $\exp(j\phi'''(0)\tau^3/3! + ... + j\phi^{(n)}(0)\tau^n/n! + ...)$. The LPFT forms that can be used to remove effects of the higher order derivatives from the signal phase are introduced in [7], [8]. These techniques are computationally demanding and difficult for application in the ISAR imaging in the real-time.

An alternative technique, the order adaptive LPFT, is proposed in [9]. The spectral width of the signal's FT is used as an indicator of the polynomial phase order. Namely, the proper order and parameters of the LPFT are applied if its width in the frequency domain is close to the width of considered window function $W(\omega_\tau)$.

The algorithm for the order adaptive LPFT determination can be summarized as follows:

- It begins with the ordinary FT calculation (zero-order LPFT) in the first step. If the width of this transform in the frequency domain is equal to the window width, it means that the image is already focused and there is no need for the LPFT order increase. Otherwise go to the next step.
- Use the first order LPFT form considered in this report, eq.(19). If the width of this transform in the frequency domain is equal to the window width, it means that the image is focused. If the LPFT still have some spread we should introduce a new parameter, β, into the transform (next coefficient in the LPFT phase will be $-\beta\tau^3/3!$) and repeat the operation.

This very simple idea could be used for signals with one or at most few components. In complex multicomponent signal cases, more sophisticated techniques, based on the concentration measures, will be introduced in the next section.

3.1.3 Concentration measure

From the derivations given above, it can be concluded that for a known chirp-rate parameter we can obtain a focused radar image (highly concentrated time-frequency (TF) representation). Also, it can be seen that the ISAR imaging based on the LPFT for a known chirp-rate parameter is slightly more demanding than the standard ISAR imaging since, in addition to the standard procedure, it requires multiplication with the term $\exp(-j\alpha\tau^2/2)$. The next question is how to determine a value of the parameter α that will produce highly concentrated images. There are several methods in the open literature. Here, the concentration measures will be used [10, 11, 12]. Before we propose our concentration measure, some properties of the LPFT will be reviewed. The LPFT satisfies the energy conservation property:

$$\int_{-\infty}^{\infty} |F(\omega_\tau, m; \alpha)|^2 d\omega_\tau = \int_{-\infty}^{\infty} F(\omega_\tau, m; \alpha) F^*(\omega_\tau, m; \alpha) d\omega_\tau$$

$$= \int_{-\infty}^{\infty}\int_{-\infty}^{\infty}\int_{-\infty}^{\infty} q(m,\tau_a)w(\tau_a)\exp(-j\alpha\tau_a^2/2)\exp(-j\omega_\tau\tau_a)\times$$
$$q^*(m,\tau_b)w(\tau_b)\exp(j\alpha\tau_b^2/2)\exp(j\omega_\tau\tau_b)d\tau_a d\tau_b d\omega_\tau$$
$$= \int_{-\infty}^{\infty}\int_{-\infty}^{\infty} q(m,\tau_a)w(\tau_a)\exp(-j\alpha\tau_a^2/2)\times$$
$$q^*(m,\tau_b)w(\tau_b)\exp(j\alpha\tau_b^2/2)\delta(\tau_a-\tau_b)d\tau_a d\tau_b$$
$$= \int_{-\infty}^{\infty} |q(m,\tau)|^2 w^2(\tau)d\tau. \tag{25}$$

Consider now the measure $\int_{-\infty}^{\infty}|F(\omega_\tau,m;\alpha)|^\gamma d\omega_\tau$ for $\gamma\to 0$. Assume that $F(\omega_\tau,m;\alpha)$ is concentrated in a narrow region around the origin in the frequency domain:

$$|F(\omega_\tau,m;\alpha)| = 0 \text{ for } \omega_\tau \geq \Omega/2. \tag{26}$$

Then, we obtain:

$$\lim_{\gamma\to 0}\int_{-\infty}^{\infty}|F(\omega_\tau,m;\alpha)|^\gamma d\omega_\tau = \Omega. \tag{27}$$

We can see that the considered measure is smaller in the case of signals concentrated in narrower intervals in the TF plane. Therefore, this type of measure can be used to indicate concentration of the TF representation. In a realistic scenario, where signal side lobes and noise exist within the entire interval, this measure with $\gamma = 0$ cannot be used, since it will produce an approximately constant value. In order to handle this issue, we can use $0 < \gamma < 2$ instead of $\gamma = 0$. As a good empirical value in our analysis we adopted $\gamma = 1$. Accurate results can be achieved for a wider region of $\gamma \in [0.5, 1.5]$.

The concentration measure based on the above analysis can be written as:

$$H(m,\alpha;\gamma) = \frac{1}{\int_{-\infty}^{\infty}|F(\omega_\tau,m;\alpha)|^\gamma d\omega_\tau}. \tag{28}$$

Higher concentrated signals will be represented by a higher value of concentration measure (28). This concentration measure has been proposed [11], where it is analyzed in detail and compared with other concentration measures. This concentration measure produces accurate results for multicomponent signals as well.

3.1.4 Estimation of the chirp rate based on the concentration measure

Determination of the optimal chirp rate parameter, α, can be performed by a direct search of the assumed set of α values:

$$\hat{\alpha}_{opt}(m) = \arg\max_{\alpha \in \Lambda} H(m, \alpha; \gamma) \tag{29}$$

This search procedure is performed over the parameter space $\Lambda = [0, \alpha_{\max}]$, where $\alpha_{\max}$ is the chirp-rate that corresponds to the TF plane diagonal. $\alpha_{\max}$ can be written as $\alpha_{\max} = 2\pi(1/2T_s)/(NT_s/2) = 2\pi/(NT_s^2)$, where $1/2T_s$ is the maximal frequency that can be achieved with sampling rate T_s within repetition time T_r, $T_s = T_r/N$. The direct search over a single parameter is currently considered as an acceptable computational burden. However, in the case when calculation time is critical, faster procedures should be used. For example, in the case of monocomponent signals embedded in moderate noise, the LMS style algorithm can be employed. The optimal value of the chirp-rate parameter can be evaluated as:

$$\alpha_{i+1}(m) = \alpha_i(m) - \mu \frac{H(t, \alpha_i(m); \gamma) - H(t, \alpha_{i-1}(m); \gamma)}{\alpha_i(m) - \alpha_{i-1}(m)} \tag{30}$$

where $[H(m, \alpha_i(m); \gamma) - H(m, \alpha_{i-1}(m); \gamma)]/[\alpha_i(m) - \alpha_{i-1}(m)]$ is used to estimate gradient of the concentration measure and μ is the predefined step size. This form of the algorithm has been implemented and applied for TF representations in [11]. A very fast (but sensitive to noise influence) technique for estimation of the chirp-rate parameters has been proposed in [13].

3.1.5 Multicomponent signals

The previously described procedures for determination of the adaptive chirp-rate parameter can be applied when the reflected chirp can be represented as a monocomponent FM signal. Furthermore, the same procedure can be applied for multicomponent signals with the same or similar second derivatives of the signal phase, since the search for just one chirp-rate parameter needs to be performed. This situation corresponds to closely spaced scatterer points in the radar image with similar motion trajectories.

However, a modification is required in the case of several components, with different chirp-rates. In this case the previously described algorithm would produce a highly concentrated dominant signal component, while the remaining components

would be spread across the TF plane. The method proposed in [14] is based on the calculation of an adaptive transform, as a weighted sum of the LPFTs:

$$F_{AD}(\omega_\tau, m) = \frac{1}{\int_{-\infty}^{\infty} H(m,\alpha;\gamma)d\alpha} \int_{-\infty}^{\infty} F(\omega_\tau, m;\alpha) H(m,\alpha;\gamma) d\alpha \tag{31}$$

where the weighted coefficients are proportional to the concentration measure. This method had produced good results for signals with components of similar magnitudes. However, if signal components significantly differ in amplitude, the results are not satisfactory. Namely, signal components with smaller amplitude would be additionally attenuated. In order to avoid this drawback, we will use the following adaptive local polynomial FT:

$$F_{AD}(\omega_\tau, m) = \sum_{i=1}^{P} F(\omega_\tau, m; \alpha_i(m)) \tag{32}$$

where the first adaptive frequency is estimated as:

$$\alpha_1(m) = \arg\max_{\alpha} H^{(0)}(m,\alpha;\gamma) \tag{33}$$

with $H^{(0)}(m,\alpha;\gamma) = H(m,\alpha;\gamma)$, given with (28) and set $i = 1$. After detection of the first component's chirp-rate, values of $H(m,\alpha;\gamma)$ in a narrow zone around $\alpha_1(m)$ are neglected, and the search for the next maximum is performed. Each iteration in this procedure could be described into two steps:

$$H^{(i)}(m,\alpha;\gamma) = \begin{cases} H^{(i-1)}(m,\alpha;\gamma) & |\alpha - \alpha_i(m)| \geq \Delta \\ 0 & \text{otherwise} \end{cases} \tag{34}$$

$$\alpha_{i+1}(m) = \arg\max_{\alpha} H^{(i)}(m,\alpha;\gamma), i = i+1.$$

This procedure should be stopped after the maximal value of $\arg\max_\alpha H^{(i)}(m,\alpha;\gamma)$ becomes smaller than an assumed threshold. We set that the threshold is 25% of $\max_\alpha H^{(0)}(m,\alpha;\gamma)$, i.e., 25% of concentration measure before we start with peeling off components. Note that the parameter Δ should be selected carefully so that the next recognized component is not just a "side lobe" of the previous strong component. In the case when components have chirp-rates close to each other, it is enough to recognize a single chirp-rate, since the proposed approach will improve concentration of all the components with similar chirp-rates. In our experiments we

assumed that the number of components with different chirp-rates for considered radar chirp cannot be larger than 8 and we selected that $\Delta = \alpha_{\max}/16 = \pi/(8NT_s^2)$ (see also section 3.1.4). It produces accurate results in all of our experiments. Note that an alternative method for evaluation of the LPFT is proposed in [15].

3.1.6 Combination of the results from various radar chirps

In the case of radar signals we can assume that scatterers closely spaced in the range/cross-range plane have similar motion parameters. This means that for chirps with similar chirp number we can take similar values of the chirp-rate parameter. The chirp-rate estimated for the m-th chirp can be used with a small error for the next chirp signal, without recalculating the concentration measure. This simplified technique was accurate for simple simulated reflector geometry. In the case of complex reflector geometry, with numerous closely spaced components, inaccurate chirp-rate parameter estimates are obtained for several chirps. Usage of one chirp-rate for the following chirps causes a propagation effect error. Therefore, the concentration measure must be calculated and chirp-rate parameter should be estimated for each chirp. In order to refine the results further, non-linear filtering of the obtained chirp-rates is performed. Assuming that the chirp-rate parameter $\alpha(m)$ is estimated for each chirp, the nonlinear median filter can be calculated as:

$$\hat{\alpha}(m) = \text{median}\{\alpha(m+i), i \in [-r, r]\} \tag{35}$$

where $2r + 1$ is the width of the used median filter. Note that other filters with the ability to remove impulse noise can be used here instead of the median filter, for example the α-trimmed mean filters [16, 17].

3.2 Second form: Adaptive LPFT for regions of the radar image

Methods for adaptive calculation of the radar image described so far propose evaluation of the adaptive parameter for each considered chirp and a possible refinement by combining results obtained on closely spaced scatterers. The implicit assumption was that the close points in the range/cross-range domain have similar chirp-rate parameters. In order to have a more robust technique that is able to deal with more challenging motion models, we propose an alternative form of the adaptive LPFT with 2D optimization of chirp parameters. In defining this procedure, we keep in mind that relatively small portion of the radar image is related to the target. We will consider just the part of the radar image that exceeds a threshold:

$$I_\varepsilon(\omega_\tau,\omega_m)=\begin{cases}1 & |Q(\omega_\tau,\omega_m)|>\varepsilon\max\{|Q(\omega_\tau,\omega_m)|\}\\ 0 & \text{otherwise.}\end{cases} \tag{36}$$

The region $I_\varepsilon(\omega_\tau,\omega_m)$ can be separated into non-overlapping regions:

$$I_\varepsilon(\omega_\tau,\omega_m)=\bigcup_{i=1}^{p_\varepsilon} I_i(\omega_\tau,\omega_m) \tag{37}$$

where $I_i(\omega_\tau,\omega_m)\cap I_j(\omega_\tau,\omega_m)=\emptyset$ for $i\neq j$. Note that the number of separated regions p_ε depends on selected threshold ε. By using the inverse 2D FT we can calculate signals associated with the region $I_i(\omega_\tau,\omega_m)$

$$q_i(m,\tau)=IFT\{Q(\omega_\tau,\omega_m)I_i(\omega_\tau,\omega_m)\},\quad i=1,2,...,p_\varepsilon. \tag{38}$$

Now, we can assume that signal $q_i(m,\tau)$ is generated by a single reflector. Then, we can perform optimization of each signal $q_i(m,\tau)$. Since this signal is already localized in the range/cross-range domain, we will not perform optimization for each τ or m, but only optimization with a single chirp function for each region $I_i(\omega_\tau,\omega_m)$:

$$F_i(\omega_\tau,\omega_m;\hat{\alpha}_i)=\int_{-\infty}^{\infty}\sum_{m=0}^{M-1} q_i(m,\tau)\exp(-j\hat{\alpha}_i\tau^2/2-j\omega_\tau\tau-j\omega_m m)d\tau \tag{39}$$

where

$$\hat{\alpha}_i=\arg\max_{\alpha}\frac{1}{\int_{-\infty}^{\infty}\sum_{m=0}^{M-1}|F_i(\omega_\tau,\omega_m;\alpha)|^\gamma d\omega_\tau}. \tag{40}$$

The radar image is calculated as a sum of the adaptive LPFT $F_i(\omega_\tau,\omega_m;\hat{\alpha}_i)$:

$$F_{\varepsilon,AD}(\omega_\tau,\omega_m)=\sum_{i=1}^{p_\varepsilon} F_i(\omega_\tau,\omega_m;\hat{\alpha}_i). \tag{41}$$

In our experiments we obtain very good results for ε over a relatively wide range for numerous radar images.

However, additional optimization can be done based on the threshold ε. Here, a three-step technique for threshold selection is considered. In the first stage we consider various thresholds $\varepsilon \in \Xi$ and calculate $F_{\varepsilon,AD}(\omega_\tau, \omega_m)$ for each threshold from the set. Then, we calculate the optimal LPFT as $F_{\varepsilon,AD}(\omega_\tau, \omega_m)$ that achieves the best concentration over $\varepsilon \in \Xi$. Since, by introducing the threshold value, we remove a part of the range/cross-range plane (see (36)) the energy of $F_{\varepsilon,AD}(\omega_\tau, \omega_m)$ should be normalized to the energy of signal above the specific threshold:

$$F'_{\varepsilon,AD}(\omega_\tau, \omega_m) = \frac{F_{\varepsilon,AD}(\omega_\tau, \omega_m)}{\sqrt{\int_{-\infty}^{\infty} \sum_{m=0}^{M-1} |Q(\omega_\tau, \omega_m)|^2 I_\varepsilon(\omega_\omega, \omega_m) d\omega_t}},$$

$$\hat{\varepsilon} = \arg\max_{\varepsilon \in \Xi} \frac{1}{\int_{-\infty}^{\infty} \sum_{m=0}^{M-1} |F'_{\varepsilon,AD}(\omega_\tau, \omega_m)|^\gamma d\omega_t}. \tag{42}$$

In this procedure the transforms $F_{\varepsilon,AD}(\omega_\tau, \omega_m)$, $\varepsilon \in \Xi$, are compared under unequal conditions since they are obtained with various thresholds ε and they could have different number of recognized components. The obtained adaptive transform $F_{\varepsilon,AD}(\omega_\tau, \omega_m)$ could be poorly concentrated than a particular $F'_{\varepsilon,AD}(\omega_\tau, \omega_m)$ from the considered set of ε values. However, this radar image is near-optimal and a small additional manual adaptation around the estimated $\hat{\varepsilon}$ could be performed in the third stage of this procedure to obtain the optimal image. In our experiments the obtained $\hat{\varepsilon}$ is underestimated (see Example 7). Thus, an additional search could be performed over higher values of ε.

4 Results

Several numerical examples will be presented here to justify the presented approach. Examples 1-4 are generic signals representing one received radar chirp that prove that the adaptive LPFT can be used to produce highly concentrated TF representation for the following 1D signals: linear FM, sinusoidal FM, multicomponent signal with similar chirp-rates and multicomponent signals with differing chirp-rates. Examples 5 and 6 demonstrate that the adaptive LPFT optimized for each chirp signal with filtering data produced by adjacent radar chirps gives accurate results. Example 7 illustrates the second adaptive LPFT algorithm with optimization over regions of the radar image.

4.1 Example 1

The first signal that will be considered is a linear FM signal $f(t) = \exp(j64\pi t^2/2)$ embedded in Gaussian noise with variance $\sigma^2 = 1$. The signal is sampled with $\Delta t = 1/128$sec. The FT of the windowed signal with a Hanning window of the width $T = 2$ sec is shown in Figure 2a. It can be seen that the FT is spread. Thus, if this signal is a part of the received signals reflected from a target, we will obtain a defocused radar image. Results obtained with narrower Hanning windows are given in Figure 2b. The improvement could be observed from this figure, but generally speaking it is slight. The concentration measure (28) for $\gamma = 1$ is presented in Figure 2c, with marked detected chirp-rate parameter. Finally, the adaptive LPFT is given in Figure 2d calculated for parameter α for which the concentration measure given in Figure 2c is maximized. The significant improvement achieved by the LPFT is obvious.

4.2 Example 2

The second signal is a more complex sinusoidal FM signal: $f(t) = \exp(j16\sin(2\pi t))$. The signal sampling and noise environment are the same as in Example 1. The FTs with a wide and a narrow window around a given time instant (STFT), [18], are depicted in Figures 3a,b. This STFT illustration for a fixed instant corresponds to the radar image for considered m. It can be used to estimate the radar image depending on different chirp-rates. Again we can see that for each instance this representation is spread in frequency domain. It means that the radar image obtained based on the FT for signals of this form will be defocused. The adaptive LPFT with a single chirp-rate, calculated for each instant, is given in Figure 3c. A significant improvement is achieved. Also, it can be noticed that the representation is not ideal in the region with higher order derivatives. These derivatives can be removed by

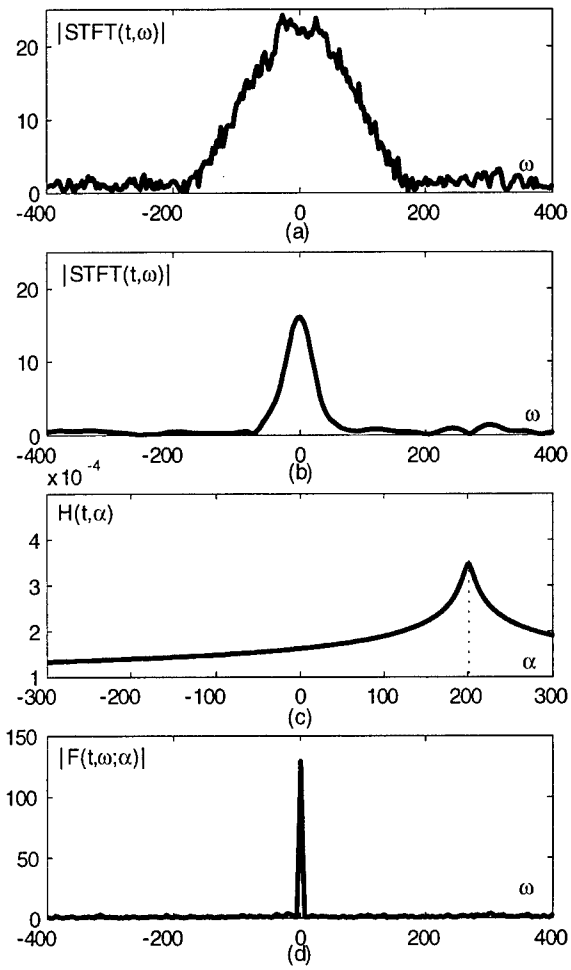

Figure 2: *Spectral analysis of the linear FM signal: (a) FT with a wide window; (b) FT with a narrow window; (c) Concentration measure; (d) Adaptive LPFT.*

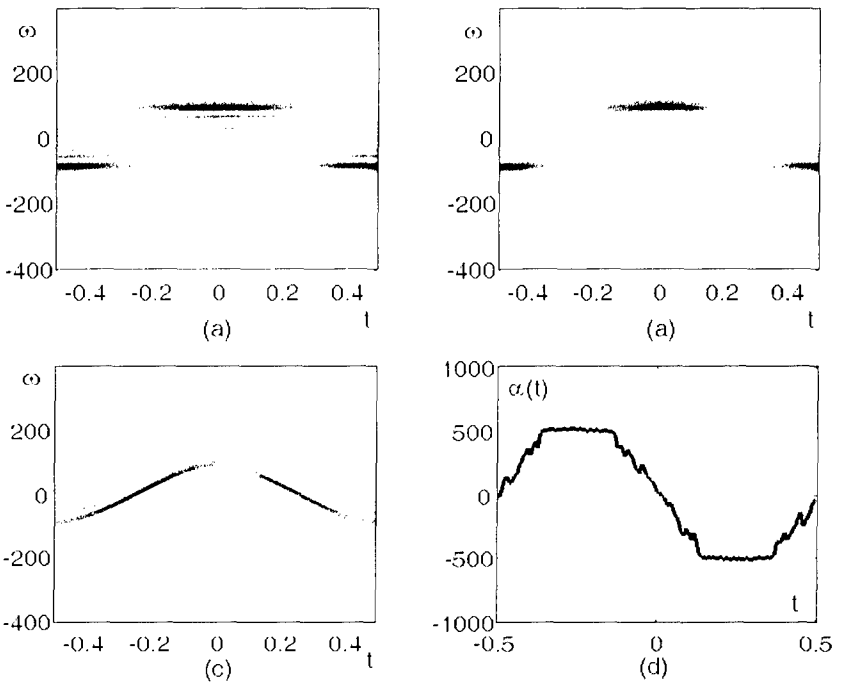

Figure 3: *Time-frequency analysis of the sinusoidal FM signal: (a) STFT with a wide window; (b) STFT with a narrow window; (c) Adaptive LPFT; (d) Adaptive chirp-rate parameter.*

employing higher order LPFT form [7]-[9]. The adaptive chirp rate is given in Figure 3d.

4.3 Example 3

A three-component signal: $f(t) = \exp(j22\pi t^2 + j48\pi t) + \exp(j32\pi t^2) + \exp(j42\pi t^2 - j48\pi t)$ is considered next. The STFT with a wide and a narrow window is given in Figure 4a,b. The adaptive LPFT calculated as in the case of monocomponent signal is given in Figure 4c. It can be seen that the concentration is improved for all three components. The component in the middle is enhanced the best, but other components with similar chirp rates are also improved. The adaptive parameter is given in Figure 4d. This case corresponds to a signal obtained from several scatterers in the same cross-range with similar chirp-rates. The difference in chirp-rates of these components in fact is not so small, it is 30% of the chirp-rate of the middle component. In real-time applications it represents a realistic scenario of the scatterers in the radar image. We can see that the concentration of all components is satisfactory. It can also be seen that accuracy of this procedure is not affected by the distance between scatterers. The same accuracy is achieved for the left part of Figure 4c, where we assume that scatterers are far from each other, as well as in the right part of this illustration, where it can be assumed that scatterers are close to each other.

4.4 Example 4

A three-component signal: $f(t) = \exp(j11\pi t^2 + j48\pi t) + \exp(j32\pi t^2) + \exp(j67\pi t^2 - j48\pi t)$ is considered. However, in this case the chirp-rates of components are quite different (difference between chirp-rates is more than 60% of chirp-rate of the middle component). The STFT is given in Figure 5a, while the "adaptive" transform, assuming the signal has a single chirp-rate, is given in Figure 5b. It can be seen that in each instant, the transform is adjusted to one component, while other components remain spread. For $t < 0.3$ the LPFT is highly concentrated for the middle component, but when components are close to each other (corresponding to closely spaced scatterers) the adaptive chirp-rate switches several times between components. The adaptive weighted LPFT (32) is given in Figure 5c. It can be seen that all components have improved concentration and that concentration is not influenced by the distance between scatterers. The detected adaptive chirp-rates are given in Figure 5d.

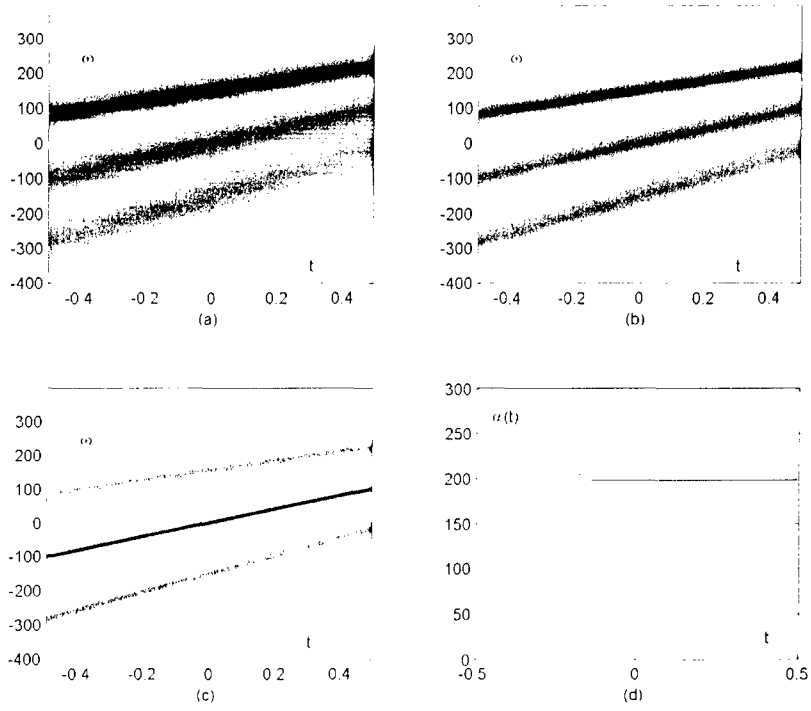

Figure 4: *Time-frequency analysis of the multicomponent signal: (a) STFT with a wide window; (b) STFT with a narrow window; (c) Adaptive LPFT; (d) Adaptive chirp-rate parameter.*

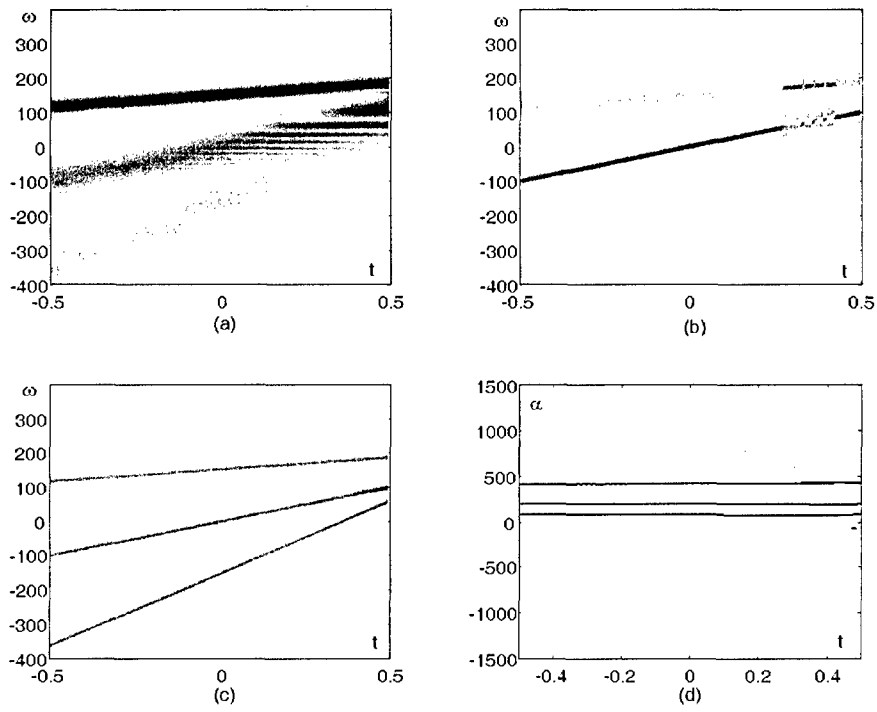

Figure 5: *Time-frequency analysis of the multicomponent signal: (a) STFT with a wide window; (b) LPFT with a single chirp parameter estimated in each instant; (c) Weighted adaptive LPFT; (d) Estimated chirp rates.*

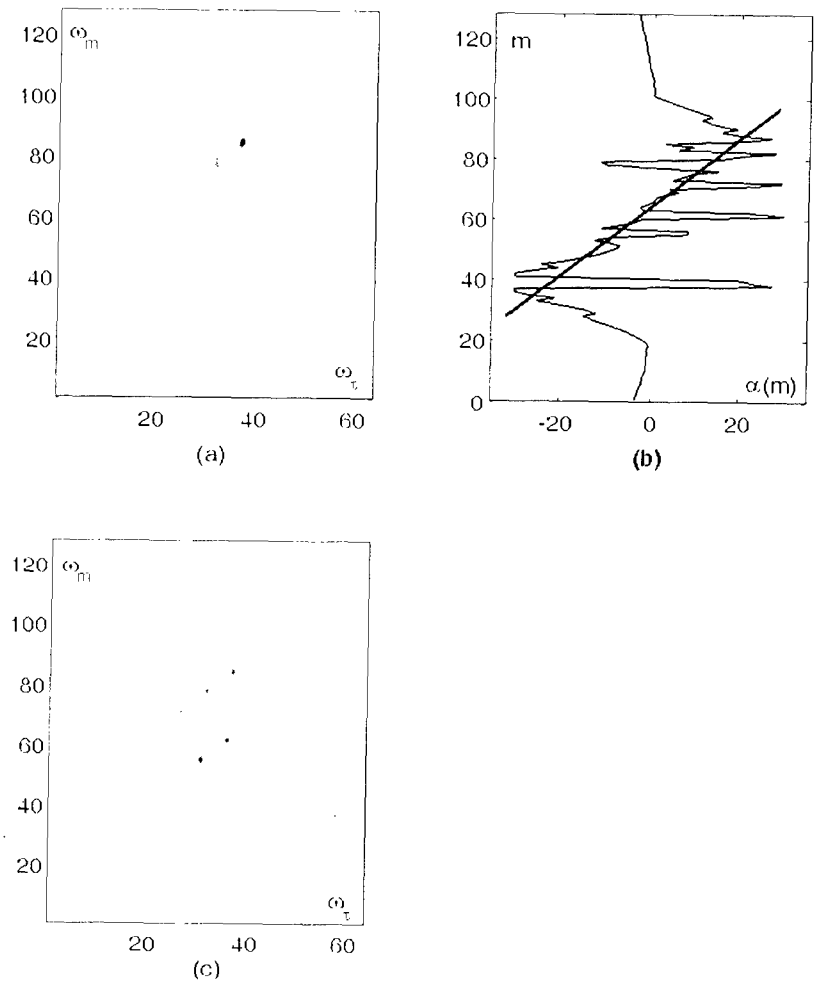

Figure 6: *Simulated radar image: (a) Results obtained by the FT; (b) Adaptive chirp-rate parameter as function of m (thick line is linear approximation); (c) Radar image based on the adaptive LPFT.*

4.5 Example 5

The simulated radar target setup according to the experiment in [4] is considered. The reflectors are at the positions $(x, y) = \{(-2.5, 1.44), (0, 1.44), (2.5, 1.44), (1.25, -0.72), (0, 2.88), (-1.25, 0.72)\}$ in meters. The high resolution radar operates at the frequency $f_0 = 10.1$GHz, with a bandwidth of linear FM chirps $B = 300$MHz and pulse chirp repetition time $T_r = 15.6$ms. The target is at 2km distance from the radar, and rotates at $\omega_R = 4^0/\sec$. The nonlinear rotation with frequency $\Omega = 0.5$Hz and amplitude $A = 1.25^0/\sec$ is superimposed, $\omega_R(t) = \omega_R + A\sin(2\pi\Omega t)$. The FT based image of the radar target is depicted in Figure 6a. The radar image obtained by using the adaptive LPFT calculated for each chirp separately is presented in Figure 6c, while the adaptive parameter for each chirp-signal is given in Figure 6b. It can be seen that the adaptive parameter linearly varies between the limits of the target. However, the impulse like errors in the estimation of the chirp-rate can be observed from Figure 6b. It suggests that the improvement of the results can be achieved by filtering chirp-rate parameters.

4.6 Example 6

In this example we consider simulated Boeing-727 radar data. The FT based image is presented in Figure 7a. It can be seen that the radar image is defocused. However, the radar imaging based on the adaptive LPFT determined for each radar chirp produces a significant improvement in the signal representation, Figure 7b. In order to obtain better results for closely spaced reflectors, we consider the adaptive chirp-rate parameter depicted in Figure 7c as a dotted line. We expected that removing impulse like disturbances will produce better results. To this aim, the median filtering of the adaptive parameter is performed. In order to evaluate the outcome, the linear interpolation of estimated chirp-rates is performed (The linear interpolation is depicted with thick line in Figure 7c). The result obtained with these parameters is depicted in Figure 7d. It is better than its counterpart in Figure 7b except for the nose reflectors. A possible reason is the fact that the received signal corresponding to these scatterers can have higher order polynomials in the signal phase. The higher order LPFT forms [7]-[9] could be used for these scatterers (see Section 3.1.2).

4.7 Example 7

In this example we consider the same target as in Example 5. The main difference in this example is the complex motion pattern that cannot be modeled with just a rotation. The radar image calculated by using the 2D FT is presented in Figure 8a. Region-of-interest $I_\varepsilon(\omega_\tau, \omega_m)$ is determined by (36) with the threshold set to

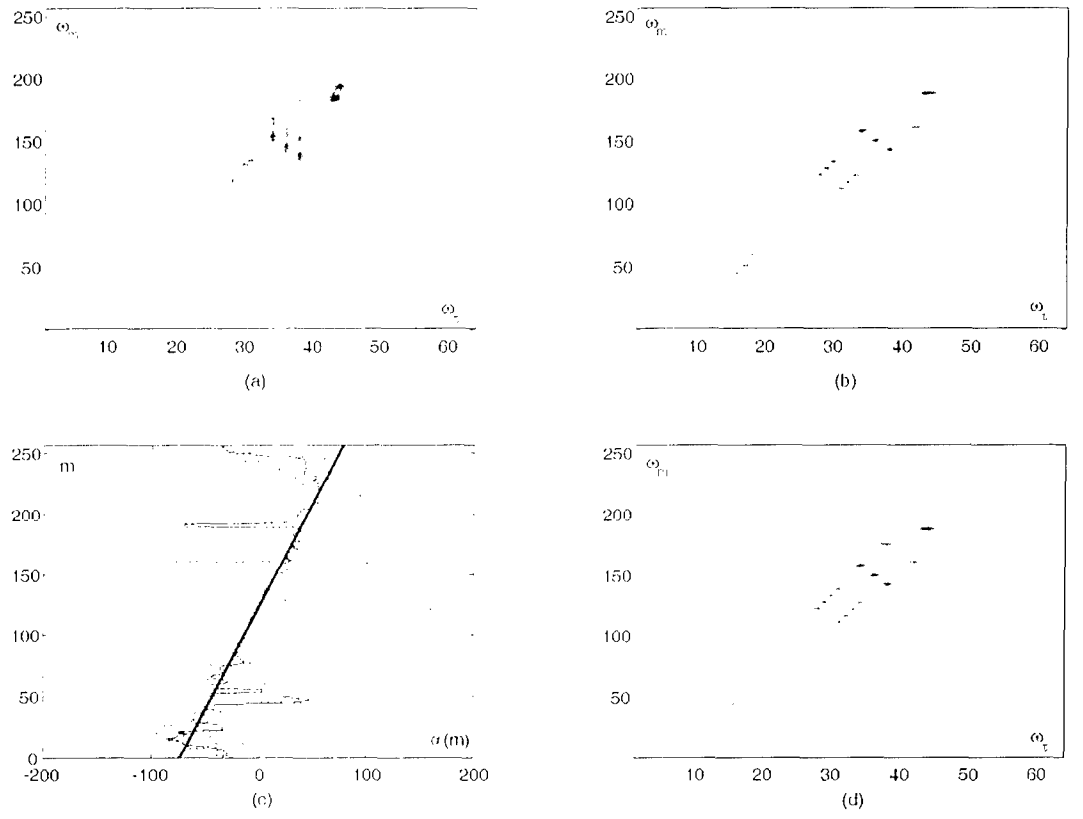

Figure 7: *B727 radar image: (a) Results obtained by the FT based method; (b) Adaptive LPFT method; (c) Adaptive chirp-rate - dotted line; Filtered adaptive chirp-rate - dashed line; Linear interpolation of filtered data - solid line; (d) Adaptive LPFT with interpolated data.*

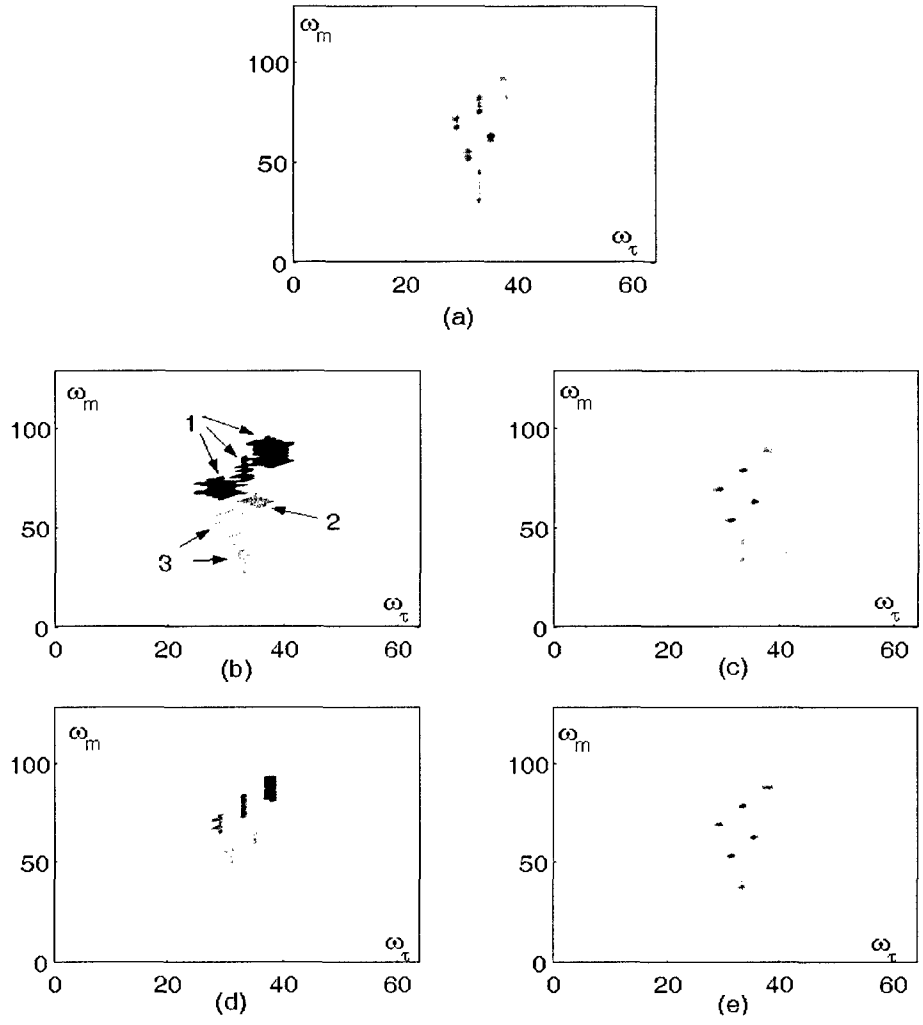

Figure 8: *Simulated radar image with complicated motion pattern: (a) Results obtained by the FT; (b) Regions of interest* $I_{\varepsilon=0.05}(\omega_t, \omega_m)$ *with three recognized separated regions; (c) Adaptive LPFT based on region optimization with* $\varepsilon = 0.05$, $F_{\varepsilon=0.05}(\omega_t, \omega_m)$*; (d) Regions of interest* $I_{\varepsilon=0.20}(\omega_t, \omega_m)$ *with six recognized separated regions; (e) Adaptive LPFT based on region optimization with* $\varepsilon = 0.20$, $F_{\varepsilon=0.20}(\omega_t, \omega_m)$.

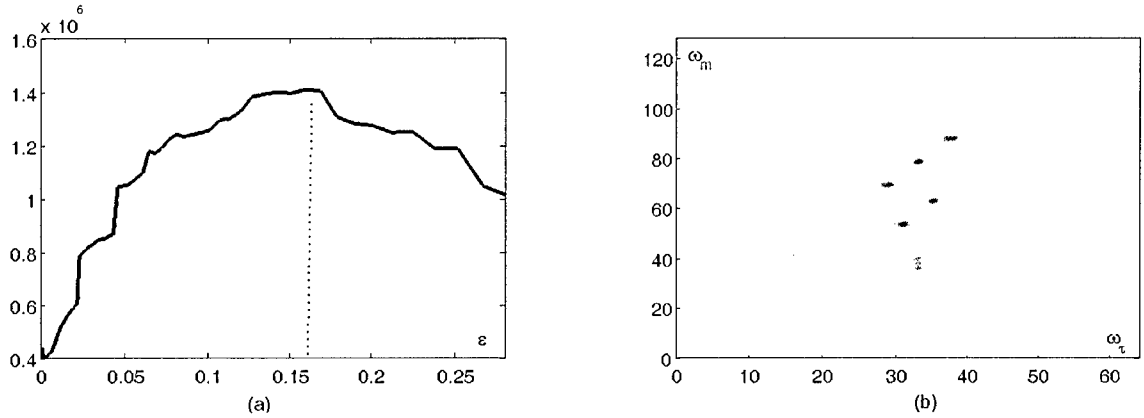

Figure 9: *Adaptive LPFT with adaptive threshold: (a) Concentration measure for various threshold levels. Optimal threshold value is depicted with dashed line. (b) Adaptive LPFT with adaptive threshold.*

$\varepsilon = 0.05$. Three separated regions are detected in the radar image, denoted in Figure 8b, in different shades of gray. The region denoted with 1 corresponds to three radar scatterers. Since these three scatterers move in a similar manner, the concentration of these components is significantly improved (see Figure 8c) with respect to the radar image calculated with 2D FT. The region denoted with number 3 corresponds to two radar scatterers. In this case, the concentration of one of the components from the region is improved, while the other component remains spread. The reason is in fact that these scatterers move in a quite different manner. When we apply threshold $\varepsilon = 0.2$, we obtain 6 regions of interest that correspond to 6 radar scatterers (Figure 8d). The resulting radar image is focused for all scatterers (Figure 8e). The threshold ε could be set in an empirical manner. However, a procedure for threshold optimization could be very helpful. The concentration measure of the adaptive LPFT for various threshold levels is depicted in Figure 9a and the obtained value in the optimization procedure is $\hat{\varepsilon} \approx 0.155$. The LPFT form with adaptive threshold is shown in Figure 9b. It can be seen that the radar image obtained in Figure 9b is slightly worse than the radar image with additionally adjusted threshold Figure 8e.

5 Conclusion

The adaptive local polynomial Fourier transform based method for enhancement of defocused radar images has been proposed. The adaptive parameters in the transform are obtained by using a simple concentration measure. For monocomponent and multicomponent signals with similar chirp-rates, a single chirp-rate parameter is estimated for each chirp. For multicomponent signals with different chirp-rates, an adaptive weighted local polynomial FT should be employed. It has been shown that the ISAR images could be improved by combining results achieved from various chirps. For targets with very complex motion pattern, the separation of the radar image in regions-of-interests and optimization of the radar signal within regions is proposed. The proposed technique does not assume any particular model of radar target motion. It can be applied for any realistic motion of targets.

References

1. Y. Wang, H. Ling, V. C. Chen: "ISAR motion compensation via adaptive joint time-frequency techniques," *IEEE Trans. Aer. Ele. Sys.*, Vol. 34, No. 2, Apr. 1998, pp. 670-677.

2. S. Barbarossa, A. Scaglione, G. B. Giannakis: "Product high-order ambiguity function for multicomponent polynomial-phase signal modeling," *IEEE Trans. Sig. Proc.*, Vol. 46, No. 3, Mar. 1998, pp. 691-708.

3. A. Quinquis, C. Ioana, E. Radoi: "Polynomial phase signal modeling using warping-based order reduction," in *Proc. of ICASSP '04*, Vol. 2, May 2004, pp. 741-744.

4. S. Wong, E. Riseborough, and G. Duff: "Experimental investigations on the distortion of ISAR images using different radar waveforms," Defence R&D Canada - Ottawa, DRDC Ottawa TM 2003-196, 2003.

5. S. Wong, E. Riseborough, and G. Duff: "Distortion in the ISAR (inverse synthetic aperture radar) images from moving targets," in *Proc. of IEEE ICIP*'2004, Vol. I, pp. 25-28, 2004.

6. T. Thayaparan, G. Lampropouols, S. K. Wong and E. Riseborough, "Application of adaptive joint time-frequency algorithm for focusing distorted ISAR images from simulated and measured radar data," *IEE Proc. Radar Sonar Navig.*, Vol. 150, No. 4, Aug. 2003, pp. 213-220.

7. V. Katkovnik, "A new form of the Fourier transform for time-frequency estimation," *Sig. Proc.*, Vol. 47, No. 2, pp. 187-200, 1995.

8. V. Katkovnik, "Local polynomial periodogram for time-varying frequency estimation," *South Afr. Stat. Jour.*, Vol. 29, No. 2, pp. 16, 168-195.

9. LJ. Stanković, S. Djukanović, "Order adaptive local polynimial FT based interference rejection in spread spectrum communicaton systems," in *Proc. of IEEE WISP 2003.*

10. R. G. Baraniuk, P. Flandrin, A. J. E. M. Jensen, O. J. J. Michel, "Measuring time-frequency information content using Rényi entropy," *IEEE Trans. Inf. Th.*, vol. 47, no. 4, May 2001, pp. 1391-1409.

11. LJ. Stanković, "A measure of some time-frequency distributions concentration," *Sig. Proc.*, vol. 81, no. 3, Mar. 2001, pp. 621-631.

12. T. H. Sang, W. J. Williams, "Rényi entropy and signal dependent optimal kernel design," in *Proc. ICASSP*, vol. 2, 1995, pp. 997-1000.

13. I. Djurović, LJ. Stanković: "Moments of multidimensional polynomial FT," *IEEE Sig. Proc. Let.*, Vol. 11, No. 11, Nov. 2004, pp.879-882.

14. M. Daković, I. Djurović, LJ. Stanković, "Adaptive local Fourier transform", in *Proc. of EUSIPCO'2002*, Toulouse, France, Vol.II, pp.603-606.

15. Y. Wei, G. Bi, "Efficient analysis of time-varying multi-component signals with LPTFT," *Jour. Appl. Sig. Proc.*, No. 8, 2005, pp. 1261-1268.

16. I. Pitas, A. N. Venetsanopoulos, *Nonlinear digital filters: Principles and applications*, Kluwer Academic, 1990.

17. I. Djurović, LJ. Stanković, J. F. Böhme, "Robust L-estimation based forms of signal transforms and time-frequency representations," *IEEE Trans. Signal Processing*, Vol. 51, No. 7, July 2003, pp.1753-1761.

18. J. B. Allen and L. R. Rabiner, "A unified approach to short-time Fourier analysis and synthesis," *Proc. IEEE*, vol. 65, no. 11, pp. 1558-1564, Nov. 1977.

19. I. Djurović, T. Thayaparan, and LJ. Stanković, "Adaptive local polynomial Fourier transform in ISAR, *J. on Applied Signal Processing,* in press, 2006.

DOCUMENT CONTROL DATA

(Security classification of title, body of abstract and indexing annotation must be entered when the overall document is classified)

1. ORIGINATOR (the name and address of the organization preparing the document. Organizations for whom the document was prepared, e.g. Establishment sponsoring a contractor's report, or tasking agency, are entered in section 8.)

Defence R&D Canada – Ottawa
Ottawa, Ontario, Canada K1A 0Z4

2. SECURITY CLASSIFICATION (overall security classification of the document, including special warning terms if applicable)

UNCLASSIFIED

3. TITLE (the complete document title as indicated on the title page. Its classification should be indicated by the appropriate abbreviation (S,C or U) in parentheses after the title.)

Focusing ISAR Images using the Adaptive Local Polynomial Fourier Transform (U)

4. AUTHORS (Last name, first name, middle initial)

Thayaparan, Thayananthan

5. DATE OF PUBLICATION (month and year of publication of document)	6a. NO. OF PAGES (total containing information. Include Annexes, Appendices, etc.)	6b. NO. OF REFS (total cited in document)
September 2006	41	19

7. DESCRIPTIVE NOTES (the category of the document, e.g. technical report, technical note or memorandum. If appropriate, enter the type of report, e.g. interim, progress, summary, annual or final. Give the inclusive dates when a specific reporting period is covered.)

DRDC Ottawa Technical Memorandum

8. SPONSORING ACTIVITY (the name of the department project office or laboratory sponsoring the research and development. Include the address.)

Defence R&D Canada – Ottawa
Ottawa, Ontario, Canada K1A 0Z4

9a. PROJECT OR GRANT NO. (if appropriate, the applicable research and development project or grant number under which the document was written. Please specify whether project or grant)	9b. CONTRACT NO. (if appropriate, the applicable number under which the document was written)
15ec05	

10a. ORIGINATOR'S DOCUMENT NUMBER (the official document number by which the document is identified by the originating activity. This number must be unique to this document.)	10b. OTHER DOCUMENT NOS. (Any other numbers which may be assigned this document either by the originator or by the sponsor)
DRDC Ottawa TM 2006-185	

11. DOCUMENT AVAILABILITY (any limitations on further dissemination of the document, other than those imposed by security classification)

(X) Unlimited distribution
( ) Distribution limited to defence departments and defence contractors; further distribution only as approved
( ) Distribution limited to defence departments and Canadian defence contractors; further distribution only as approved
( ) Distribution limited to government departments and agencies; further distribution only as approved
( ) Distribution limited to defence departments; further distribution only as approved
( ) Other (please specify):

12. DOCUMENT ANNOUNCEMENT (any limitation to the bibliographic announcement of this document. This will normally correspond to the Document Availability (11). However, where further distribution (beyond the audience specified in 11) is possible, a wider announcement audience may be selected.)

13. ABSTRACT (a brief and factual summary of the document. It may also appear elsewhere in the body of the document itself. It is highly desirable that the abstract of classified documents be unclassified. Each paragraph of the abstract shall begin with an indication of the security classification of the information in the paragraph (unless the document itself is unclassified) represented as (S), (C), or (U). It is not necessary to include here abstracts in both official languages unless the text is bilingual).

(U) The adaptive local polynomial Fourier transform is employed for the improvement of the ISAR images in complex reflector geometry cases, as well as in cases of fast maneuvering targets. It has been shown that this simple technique can produce significantly improved results with a relatively modest calculation burden. Two forms of the adaptive LPFT are proposed. The adaptive parameter in the first form is calculated for each radar chirp. An additional refinement is performed by using the information from the adjacent chirps. The second technique is based on the determination of the adaptive parameter for different parts of the radar image. The numerical analysis demonstrates the accuracy of the proposed techniques. It is important to note that the proposed technique does not assume any particular model of radar target motion. It can be applied for any realistic motion of targets.

14. KEYWORDS, DESCRIPTORS or IDENTIFIERS (technically meaningful terms or short phrases that characterize a document and could be helpful in cataloguing the document. They should be selected so that no security classification is required. Identifiers such as equipment model designation, trade name, military project code name, geographic location may also be included. If possible keywords should be selected from a published thesaurus. e.g. Thesaurus of Engineering and Scientific Terms (TEST) and that thesaurus-identified. If it is not possible to select indexing terms which are Unclassified, the classification of each should be indicated as with the title.)

SAR
ISAR
Local Polynomial Fourier Transform
Time-Frequency Analysis
Moving Targets
Target Detection
Fourier Transform
Doppler Processing
Image Analysis

13. ABSTRACT (a brief and factual summary of the document. It may also appear elsewhere in the body of the document itself. It is highly desirable that the abstract of classified documents be unclassified. Each paragraph of the abstract shall begin with an indication of the security classification of the information in the paragraph (unless the document itself is unclassified) represented as (S), (C), or (U). It is not necessary to include here abstracts in both official languages unless the text is bilingual).

(U) The adaptive local polynomial Fourier transform is employed for the improvement of the ISAR images in complex reflector geometry cases, as well as in cases of fast maneuvering targets. It has been shown that this simple technique can produce significantly improved results with a relatively modest calculation burden. Two forms of the adaptive LPFT are proposed. The adaptive parameter in the first form is calculated for each radar chirp. An additional refinement is performed by using the information from the adjacent chirps. The second technique is based on the determination of the adaptive parameter for different parts of the radar image. The numerical analysis demonstrates the accuracy of the proposed techniques. It is important to note that the proposed technique does not assume any particular model of radar target motion. It can be applied for any realistic motion of targets.

14. KEYWORDS, DESCRIPTORS or IDENTIFIERS (technically meaningful terms or short phrases that characterize a document and could be helpful in cataloguing the document. They should be selected so that no security classification is required. Identifiers such as equipment model designation, trade name, military project code name, geographic location may also be included. If possible keywords should be selected from a published thesaurus. e.g. Thesaurus of Engineering and Scientific Terms (TEST) and that thesaurus-identified. If it is not possible to select indexing terms which are Unclassified, the classification of each should be indicated as with the title.)

SAR
ISAR
Local Polynomial Fourier Transform
Time-Frequency Analysis
Moving Targets
Target Detection
Fourier Transform
Doppler Processing
Image Analysis

Defence R&D Canada

Canada's Leader in Defence
and National Security
Science and Technology

R & D pour la défense Canada

Chef de file au Canada en matière
de science et de technologie pour
la défense et la sécurité nationale

www.drdc-rddc.gc.ca